

# Ultrastable optical, XUV and soft-x-ray clock transitions in open-shell highly charged ions

Chunhai Lyu,\* Christoph H. Keitel, and Zoltán Harman  
*Max-Planck-Institut für Kernphysik, Saupfercheckweg 1, 69117 Heidelberg, Germany*  
 (Dated: May 17, 2023)

Highly charged ions (HCIs) are insensitive to external perturbations and are attractive for the development of ultrastable clocks. However, only a few HCI candidates are known to provide optical clock transitions. In this Letter, we show that, as a result of strong relativistic effects, there are more than 100 suitable optical HCI clock candidates in more than 70 elements. Their transitions are embedded in the fine-structure splitting of the  $nd^4$ ,  $nd^5$  and  $nd^6$  ground-state configurations with  $n = 3, 4, 5$  being the principal quantum numbers. The corresponding high multipolarity transitions in these ions have lifetimes and quality factors many orders of magnitude longer and larger, respectively, than those in state-of-the-art clocks. Their polarizabilities are also orders of magnitude smaller, rendering them more stable against external electromagnetic fields. Furthermore, within the same electronic configurations, the clock transitions in heavy ions scale up to the XUV and soft-x-ray region, thus enable the development of clocks based on shorter wavelengths. The existence of multiple clock transitions in different charge states of a single element, as well as in a whole isoelectronic sequence, would significantly enrich the detection of fine-structure constant variations, the search for new physics and the test of nuclear theories via high-precision spectroscopy.

High-precision optical clocks have wide applications in fields such as the new definition of time units [1–3], the test of variations of the fine-structure constant [4–6], and the constrain of a conjectured fifth force [7–9] and other new physics phenomena [10, 11]. The elements of these clocks are either neutral atoms or singly charged ions [12] based on hyperfine-induced  $ns^2 \ ^1S_0 - nsnp \ ^3P_0$  [13–18] and electric quadrupole  $(n+1)s \ ^1S_{1/2} - nd \ ^2D_{5/2}$  transitions [19–23] with a quality factor  $Q = \nu/\Delta\nu$  in the range of  $10^{14} \sim 10^{17}$ . Here,  $n$  is the principal quantum number,  $\nu$  the transition frequency and  $\Delta\nu$  the corresponding natural linewidth. For specific cases such as  $\text{Lu}^+$  and  $\text{Yb}^+$ , electric quadrupole and octupole transitions between  $6s^2 - 6s5d$  [24, 25] and between  $4f^{13}6s^2 - 4f^{14}6s$  [26, 27] with  $Q$  factor in the range of  $10^{21}$  and  $10^{23}$ , respectively, are also employed.

Nevertheless, these clocks suffer from large systematic shifts and uncertainties induced by black body radiation [28, 29] and external trapping fields [12, 30]. To overcome these difficulties, clocks based on a nuclear transition in the  $^{227}\text{Th}$  isomer [31–33] and electronic transitions in highly charged ions (HCIs) [34–37] are put forward as they bear smaller polarizabilities and are sensitive to  $\alpha$  variations. While the radioactive  $^{227}\text{Th}$  nuclear clock, with  $Q = 2 \times 10^{20}$ , is still to be implemented for a direct laser excitation [38], a HCI clock based on  $\text{Ar}^{13+}$  with a modest  $Q = 4 \times 10^{13}$  has already been demonstrated via quantum logic spectroscopy [35].

One category of HCI candidates are based on hyperfine transitions of the  $1s$  electron in hydrogenlike ions [39, 40]. This transition has an energy of  $6 \mu\text{eV}$  for the hydrogen atom, but scales up to 1.4 eV (886 nm) for ions as heavy as  $^{207}\text{Pb}^{81+}$ . The second variety of HCI clock transitions are from fine-structure splittings of  $np$  valence electron

systems [41–44]. Though these ions have polarizabilities many orders of magnitude smaller than neutral atoms or singly charged ions, their clock transitions are of magnetic dipole transitions with  $Q \sim 10^{13}$  [35, 40]. Thus, one needs a long interrogation time to achieve high accuracy. Another type of HCI candidates comes from level crossings between the  $4f - 5s$  [45–47],  $4f - 5p$  [48–50], and  $5f - 6p$  [51, 52] orbitals. However, only a small number of ions close to the crossing points would provide optical clock transitions, not to mention that the close lying orbitals usually induce large polarizabilities [41, 53].

In this Letter, we put forward a category of ultrastable HCI clocks that possess  $Q$  factors beyond  $10^{23}$  and electric polarizabilities in the range of  $10^{-42} \text{ J m}^2/\text{V}^2$ . As shown in Fig. 1, the clock transitions come from fine-structure splittings in ions with one of the open-shell  $nd^4$ ,  $nd^5$  and  $nd^6$  ground-state configurations. These configurations have tens of terms with total angular momenta ranging from  $J = 0$  and  $1/2$  to  $J = 6$  and  $13/2$ . For light ions, the energy levels order linearly according to the values of the total angular momentum, and thus the lifetimes of the excited states are dominated by  $M1$  transitions to  $J \pm 1$  states. These forbidden transitions have

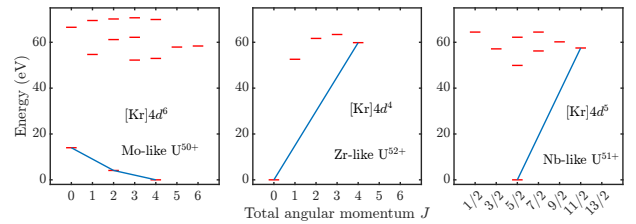


Figure 1. Low-lying levels of (a)  $\text{U}^{50+}$ , (b)  $\text{U}^{52+}$  and (c)  $\text{U}^{51+}$  ions. Clock transitions are depicted by blue lines. Similar level structures exist for  $[\text{Ar}]3d^m$  and  $[\text{Xe}]4f^{14}5d^m$  ( $m = 4, 5, 6$ ) ions.

\* chunhai.lyu@mpi-hd.mpg.de

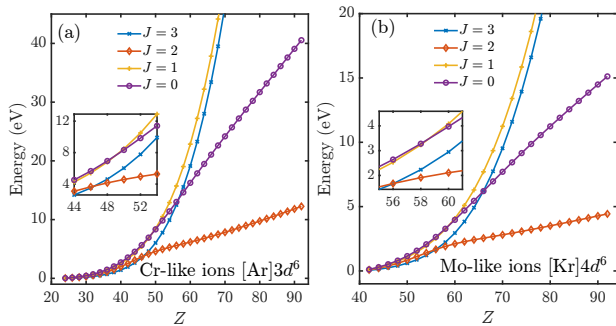


Figure 2. Excitation energies of the  $nd^6 \ ^5D_{3,2,1,0}$  state in (a) Cr- and (b) Mo-like ions as functions of atomic number  $Z$ . With a ground state of  $^5D_4$ , term reordering leads to two clock states with  $J = 2$  and  $J = 0$ , respectively. Insets are the enlarged depiction around the crossing points.

found numerous applications in the diagnostics of astrophysical and laboratory plasma properties [54–56]. However, for heavy ions which are also highly charged, the strong relativistic influence leads to a reordering of the terms and renders it possible to obtain ultrastable clocks based on high-multipolarity  $E2/M3$  forbidden transitions.

For the case of  $nd^6$ , optical clock transitions exist throughout the whole isoelectronic sequences up to  $U^{68+}$ ,  $U^{50+}$  and  $U^{18+}$  for  $n = 3, 4, 5$ , respectively, providing nearly a *hundred* of HCI clocks. Some HCIs, such as  $U^{68+}$ , might be challenging to produce, but in principle can be obtained within an electron beam ion trap [57] or a HITRAP [58]. High-precision spectroscopy of these transitions would enable an accurate determination of nuclear parameters for more than 70 elements and their isotopes ranging from  $^{46}\text{Ti}$  to  $^{238}\text{U}$  and beyond, and test state-of-the-art nuclear theories [59–63]. For  $nd^4$  and  $nd^5$ , tens of optical clock transitions also exist in light elements, but the transition energies scale up to the XUV and soft-x-ray region for heavy elements. Considering that the stability of optical lasers is approaching the fundamental limit set by thermal fluctuations of reference cavities [64–67], clocks based on lasers with shorter wavelengths [68, 69] would be one of the approaches to further improve the clock performance. Furthermore, most of these ions also have more than two clock transitions with distinct sensitivities to the variation of  $\alpha$ , rendering them good candidates for the test of new physics beyond the standard model [10].

*MCDHF-RCI calculations* — To accurately predict the transition energies and lifetimes of these clock states, we employ *ab initio* fully relativistic multiconfiguration Dirac–Hartree–Fock (MCDHF) and configuration interaction (RCI) methods implemented in the GRASP2018 codes [70, 71]. Within this scheme, the many-electron atomic state functions (ASFs) are expanded as a linear combination of configuration state functions (CSFs) which are  $jj$ -coupled Slater determinants of one-electron orbitals. The radial wavefunction for each orbital is ob-

Table 1. Predicted transition energy  $\hbar\omega$ , lifetime  $\tau$ , sensitivity to  $\alpha$  variations  $K$ , and differential polarizability  $\Delta\alpha_{eg}$  ( $10^{-40} \text{ J m}^2/\text{V}^2$ ) of clock states in selected  $[\text{Kr}]4d^6$  ions.

ions	$ e\rangle$	$\hbar\omega$ (eV)	$\tau$ (s)	$K$	$\Delta\alpha_{eg}$
$\text{Ce}^{16+}$	$^3D_2$	1.70(1)	1156	−0.55	−0.22
	$^3P_0$	3.23(1)	602	−1.50	−0.45
$\text{Dy}^{24+}$	$^3D_2$	2.20(1)	545	0.06	−0.10
	$^3P_0$	5.98(2)	11.7	−1.02	−0.20
$\text{W}^{32+}$	$^3D_2$	2.67(1)	332	0.01	−0.05
	$^3P_0$	8.69(3)	1.63	−0.61	−0.10
$\text{Pb}^{40+}$	$^3D_2$	3.23(1)	208	0.05	−0.031
	$^3P_0$	11.25(4)	0.58	−0.38	−0.062
$\text{U}^{50+}$	$^3D_2$	3.99(1)	125	0.07	−0.017
	$^3P_0$	14.31(4)	0.27	−0.23	−0.035

tained via solving the self-consistent MCDHF equations under the Dirac–Coulomb Hamiltonian. Then, the RCI method is applied to account for corrections arising from mass shift, quantum electrodynamic and Breit interactions.

For the low-lying states in  $nd^6$ ,  $nd^4$  and  $nd^5$ , the scaling of their excitation energies with respect to the atomic number  $Z$  are plotted in Figs. 2–4, respectively, where a clear reordering of the levels is observed. These values are obtained via simple calculations that only account for correlation effects within the corresponding ground-state configurations. However, for specific ions where accurate values are needed, such as the ions around the crossing points discussed below and the ions shown in Table 1, large-scale calculations with millions of CSFs are performed. This is obtained by allowing single and double excitations from the  $ns$ ,  $np$ , and  $nd$  orbitals up to the  $8k$  orbitals. As a consequence, the calculated energies and lifetimes bear a relative accuracy of 0.5% and 20%, respectively [72]. Increasing the size of the CSF basis set systematically shifts the values of the excitation energies depicted in Figs. 2–4 downward by up to 10%, but has little effects on the crossing points of the levels.

*nd<sup>6</sup> ions* — For ions in this configuration, there are 34 atomic states with total angular momentum ranging from  $J = 0$  to 6, with a  $^5D_4$  term being the ground state. In light ions, the corresponding low-lying excited states are  $^5D_{3,2,1,0}$ , respectively, and decay via  $M1$  transitions. Usually, the energies of the fine-structure multiplet scale with  $Z^2$  [34], which is the case for  $J = 1, 3$  shown in Fig. 2. However, for heavy elements, strong relativistic effects leads to large splitting between the  $nd_{3/2}$  and  $nd_{5/2}$  relativistic orbitals (the subscripts are the corresponding single-electron total angular momenta). As a consequence, the ASFs for states  $J = 0, 2$  become dominated by the  $nd_{3/2}^4 nd_{5/2}^2$  configuration [73], and their energies only increase linearly with respect to  $Z$ , and become the first two excited states. These two levels decay via slow  $E2$  transitions and thus represent the two clock states illustrated in Fig. 1(a). We notice that a similar unusual scaling of the fine-structure splittings also allows

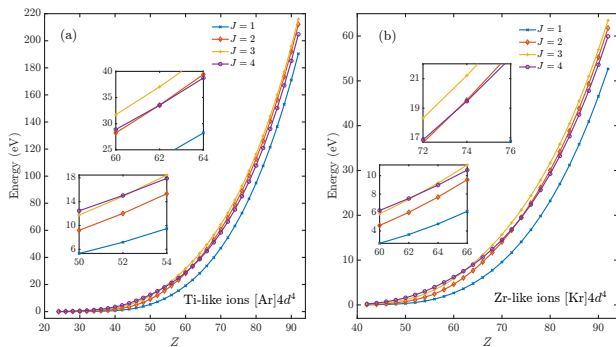


Figure 3. Excitation energies of the  $nd^4 \ ^5D_{1,2,3,4}$  states in (a) Ti- and (b) Zr-like ions as functions of atomic number  $Z$ . Term reordering leads to long-lived  $J = 4$  state. Insets are the enlarged depiction around the crossing points.

clock transitions in low charged, so-called group-16-like ions [74–76].

For Mo-like ions ( $[\text{Kr}]4d^6$ ) shown in Fig. 2(b), the level reordering of the  $J = 2$  state happens at  $\text{Ba}^{14+}$ . The transition energy between  $^5D_4$  and  $^3D_2$  is around 1.70 eV for  $\text{Ce}^{16+}$ , and scales up to 3.99 eV for  $\text{U}^{50+}$ . With a lifetime of 625 and 63 s for the two ions (see Table 1), respectively, these transitions have a  $Q$  factor of  $1.6 \times 10^{18}$  and  $3.8 \times 10^{17}$ , respectively, which are orders of magnitude higher than those in current optical clocks [13–23]. Particularly, they are more than 4 orders of magnitude higher than the first HCI clock based on  $\text{Ar}^{13+}$  [40, 43]. Thus, this isoelectronic system would contain more than 36 ion candidates suitable for optical HCI clocks operating at various wavelengths.

For Cr-like ions ( $[\text{Ar}]3d^6$ ) as presented in Fig. 2(a), the  $J = 2$  metastable state starts to emerge from  $\text{Pd}^{22+}$ . As the electrons are more tightly bound, the transition energies are relatively larger than those in Mo-like ions but are still accessible for optical lasers. Specifically, the corresponding transition energy and lifetime are 3.78 eV and 437 s, respectively, for  $\text{Cd}^{24+}$ , and scale to 11.4 eV and 18.3 s, respectively, for  $\text{U}^{68+}$ . This corresponds to  $Q$  factors around  $10^{18}$  for more than 46 optical HCI clocks in this isoelectronic sequence.

Furthermore, the second metastable state (labelled by  $J = 0$ ) lies 3.23–14.3 eV and 6.75–38.6 eV above the ground state for Mo- and Cr-like ions, respectively. While it decays to the ground state via a highly forbidden  $E4$  transition, its lifetime is dominated by an  $E2$  transition to the  $J = 2$  excited state and ranges from 64 ms to 800 s. As shown in Table 1, this  $J = 0$  state is much more sensitive to the variation of the fine-structure constant than that of the  $J = 2$  state. Taking the Mo-like  $\text{Dy}^{24+}$  as an example, with the sensitivity defined by  $K = (\Delta\omega/\omega)(\alpha/\Delta\alpha)$ , one has a  $K = 0.07$  for the  $^5D_4 - ^3D_2$  transition, but a  $K = -1.02$  for the  $^5D_4 - ^3P_0$  transition. Though the absolute sensitivities are smaller in comparison to some clock transitions near level crossings [45–52], the distinct  $\alpha$  disproportionality of two clock

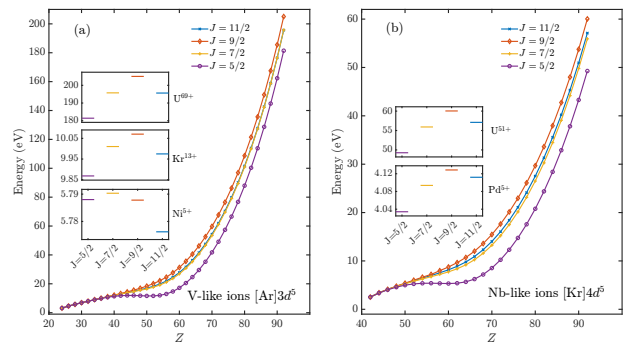


Figure 4. Excitation energies of the  $nd^5 \ ^4G_{5/2,7/2,9/2,11/2}$  states in (a) V- and (b) Nb-like ions as functions of atomic number  $Z$ . Term reordering leads to long-lived  $J = 11/2$  state. Insets are level structures of given ions.

transitions in a single ion would largely reduce systematic uncertainties in detecting  $\alpha$  variations. Similar dual-clock transitions also exist in  $\text{Yb}^+$  [5, 6], which provides the current most stringent constraint of  $\alpha$  variations. Nevertheless, one of the clock states in  $\text{Yb}^+$  has a lifetime of only 7.3 ms ( $Q = 2.2 \times 10^{14}$ ) that limits further improvements.

Another advantage of these clock ions is that they are immune to external fields. This property is mainly characterized by the small static dipole polarizability defined by  $\alpha_a = \sum_{k \neq a} -3\hbar^2 f_{ka}/2m(\hbar\omega_{ka})^2$  [77] Here,  $|a\rangle$  is either the ground state  $|g\rangle$  or the excited clock state  $|e\rangle$ ,  $\hbar$  the reduced Planck constant,  $m$  the electron mass,  $f_{ka}$  the electric dipole oscillator strength of transition from  $|a\rangle$  to an intermediate state  $|k\rangle$ , and  $\hbar\omega_{ja}$  the corresponding transition energy in units of eV. The typical polarizability values for optical clocks are larger than  $10^{-40} \text{ J m}^2/\text{V}^2$  [78, 79]. However, for ions like  $\text{U}^{50+}$ , the lowest  $|k\rangle$  state is from the  $4d^5 4f$  configuration which lies 270 eV above the two clock states. Making use of the Thomas–Reiche–Kuhn sum rule  $\sum_{k \neq a} f_{ka} = N$  ( $N$  being the number of electrons in the ion) [80], one can derive  $\alpha_{e,g} < 10^{-41} \text{ J m}^2/\text{V}^2$  which are orders of magnitudes smaller in comparison to those in neutral atoms and singly charged ions. Accordingly, the differential polarizabilities  $\Delta\alpha_{eg} = \alpha_e - \alpha_g$ , as shown in Table 1, are also much smaller.

*nd<sup>4</sup> ions* — As a counterpart of the above mentioned  $nd^6$  isoelectronic systems, the  $nd^4$  ions have similar spectroscopic terms but with a reversed level ordering. As shown in Fig. 3, these ions start with  $^5D_0$  being the ground state and  $^5D_{1,2,3,4}$  being the subsequent excited states for light elements. Though the energies of all the states scale dominantly with  $Z^2$ , the  $^5D_4$  state gradually becomes lower than the  $^5D_3$  and  $^5D_2$  states and becomes a long-lived clock state shown in Fig. 1(b). Since their energies span from 9.0 to 200 eV, they can be probed with XUV frequency combs [68, 69] and are suitable for future XUV and soft-x-ray ionic clocks. The higher transition energy would further increase the  $Q$  factor to the

range of  $10^{22}$  and beyond, thus improve the short-term stability of a clock.

In the case of Zr-like ions ( $[\text{Kr}]4d^4$ ), the clock transition energy varies from 9.0 eV in  $\text{Gd}^{24+}$  to 60 eV in  $\text{U}^{52+}$ . Through  $\text{Gd}^{24+}$  to  $\text{Ta}^{33+}$ , the  $^3H_4$  state is still above the  $^5D_2$  state. Therefore, its lifetime is mainly determined by the  $E2$  transition and are of 5 hours to 20 days. With an energy of 9 to 20 eV, these clock transitions have a quality factor of  $Q = 10^{20} \sim 10^{22}$ . For heavier ions starting from  $\text{W}^{34+}$ , the  $^3H_4$  state becomes lower than the  $^5D_2$  state. Thus, the lifetime of this metastable state can be as long as tens to hundreds of years and the quality factor of the transitions would go far beyond  $10^{22}$ . Such a long lifetime makes excitation by lasers challenging, but the position of these states can be determined with a sub-eV accuracy through mass spectroscopy [72, 81]. Furthermore, the application of twisted lasers could also enhance the transition rates of such high-multipolarity transitions [82].

Similarly, for Ti-like ions with a configuration of  $[\text{Ar}]3d^4$ , the  $^3H_4$  state lies between the  $^5D_2$  and  $^5D_3$  states for ions throughout  $\text{Xe}^{32+}$  to  $\text{Pm}^{39+}$ , with a quality factor of  $Q = 10^{20} \sim 10^{23}$  for transition energies between 17.9 and 33.0 eV. When the  $^3H_4$  state becomes lower than the  $^5D_2$  state in  $\text{Sm}^{40+}$ , its lifetime again becomes as long as hundreds of years. However, for the 202-eV metastable state in  ${}_{92}\text{U}^{70+}$ , its lifetime reduces to 48 days via an  $E4$  spontaneous emission to the ground state.

*nd<sup>5</sup> ions* — For V- and Nb-like systems, the lowest few states in neutral V and Nb atoms are formed by the  $nd^4(n+1)s$  and  $nd^3(n+1)s^2$  configurations and have  $M1$  forbidden transitions. However, for the singly charged  $\text{Cr}^+$  and  $\text{Mo}^+$  ions, the  $nd^5$   $^6S_{5/2}$  term becomes the ground state. Nevertheless, the first excited state is still a long-lived  $^6D_{1/2}$  state from the  $nd^4(n+1)s$  configuration and represents a narrow near-infrared clock transition around 1.5 eV. Starting from V-like  $\text{Mn}^{2+}$  and Nb-like  $\text{Tc}^{2+}$ , the low-lying excited states become  $^4G_{11/2-5/2}$  from the  $nd^5$  configuration.

As shown in Fig. 4, for light elements, the separations between these excited states are smaller than 10 meV that even the  $M1$  decay channel are extremely slow. As a consequence, all of these states are ultrastable clock states. Especially, through V-like  $\text{Mn}^{2+}$  to  $\text{Br}^{12+}$  and Nb-like  $\text{Tc}^{2+}$  to  $\text{Ag}^{6+}$ , our MCDHF-RCI calculations show that all the  $nd^5$   $^4G$  terms have lifetimes longer than 1 s, with energies ranging from 3.0 to 9.4 eV. From  $\text{Kr}^{13+}$  to  $\text{Y}^{16+}$  and  $\text{Cd}^{7+}$  to  $\text{Sb}^{10+}$ , even though the lifetime of the  $^4G_{5/2}$  state becomes shorter than 1 s, the other three states still provide highly forbidden clock transitions for each ion in the range of 4.7 to 11.5 eV. These multiple

optical clock transitions can be employed to infer the  $\alpha$  variations and may also find applications in searching for a fifth force with a multidimensional King-plot [83].

For elements heavier than V-like  $\text{Mo}^{19+}$  and Nb-like  $\text{Xe}^{13+}$ , the energies of the excited states scale quadratically with the atomic number  $Z$  (except for slightly abnormal behaviour of the  $J = 5/2$  state). The splittings between these states are far beyond 0.1 eV, thus fast  $M1$  decay emerges. As a result, only the state with  $J = 11/2$  that decays via a slow  $E2/M3$  transition remains metastable. As shown in Fig. 1(c) for Nb-like  $\text{U}^{51+}$ , this clock state lies 57.2 eV above the ground state. With a lifetime of 8.3 days, it represents an XUV clock with  $Q = 6.3 \times 10^{22}$ . In the case of V-like  $\text{U}^{69+}$ , the transition energy scales to 197 eV. With a lifetime of 12 hours, this soft-x-ray clock transition bears a quality factor of  $Q = 1.3 \times 10^{22}$ .

We note that, such a metastable state in Nb-like  $\text{Pb}^{41+}$  [72] has been detected in a recent high-precision mass spectroscopy experiment. The measured energy agrees with our predicted 31.68(13)-eV value obtained via large-scale MCDHF-RCI calculations. With a calculated lifetime of 26 days, it represents an XUV clock transition with  $Q = 1.1 \times 10^{23}$ , and can be effectively probed with state-of-the-art XUV frequency combs [36, 68, 69, 84–87].

*5d<sup>4,5,6</sup> ions* — The above discussions also apply to Hf-, Ta-, and W-like ions through  $\text{Hg}^{6+}$  to  $\text{U}^{20+}$ . Though most of them are radioactive, the energy and lifetime of their clock state varies from 1.06 to 11.0 eV and from 2 s to 500 days, respectively, with  $Q = 10^{16} - 10^{23}$ . Particularly, the dual clock states in W-like ions, with energies of 1.06 and 1.92 eV in  $\text{Hg}^{6+}$ , and 1.70 and 5.11 eV in  $\text{U}^{18+}$ , respectively, are also disproportional to  $\alpha$  variations, with the sensitivity of the  $J = 0$  states being around  $-0.61$  to  $-1.23$ .

*Conclusion* — We have shown that there exist more than 100 ultrastable optical HCI clock candidates. They arise from fine-structure splittings in the open-shell  $nd^4$ ,  $nd^5$  and  $nd^6$  ( $n = 3, 4, 5$ ) ions, for more than 70 elements and their isotopes, ranging from  ${}^{46}_{22}\text{Ti}$  to  ${}^{238}_{92}\text{U}$  and beyond. The corresponding transitions have  $Q$  factors and polarizabilities many orders of magnitude larger and smaller, respectively, than for current optical clocks, and thus would allow for more accurate time keeping. Most of the ions have multiple clock states with opposite dependence on fine-structure constant variations. High-precision spectroscopy of these clock transitions would enrich the search for new physics beyond the standard model, as well as the test of state-of-the-art nuclear theories. Moreover, for heavy HCIs, these clock transitions also scale up to the XUV and soft-x-ray range, and could enable the construction of short-wavelength clocks. Similar clock transitions are also found in open-shell but more complicated  $4f^m$  ions [88].

[1] BACONB Collaboration, Frequency ratio measurements at 18-digit accuracy using an optical clock network, Na-

- [2] X. Zheng, J. Dolde, V. Lochab, B. N. Merriman, H. Li, and S. Kolkowitz, Differential clock comparisons with a multiplexed optical lattice clock, *Nature* **602**, 425 (2022).
- [3] T. Bothwell, C. J. Kennedy, A. Aeppli, D. Kedar, J. M. Robinson, E. Oelker, A. Staron, and J. Ye, Resolving the gravitational redshift across a millimetre-scale atomic sample, *Nature* **602**, 420 (2022).
- [4] E. Peik, B. Lipphardt, H. Schnatz, T. Schneider, C. Tamm, and S. G. Karshenboim, Limit on the present temporal variation of the fine structure constant, *Phys. Rev. Lett.* **93**, 170801 (2004).
- [5] M. Fischer, N. Kolachevsky, M. Zimmermann, R. Holzwarth, T. Udem, T. W. Hänsch, M. Abgrall, J. Grünert, I. Maksimovic, S. Bize, H. Marion, F. P. D. Santos, P. Lemonde, G. Santarelli, P. Laurent, A. Clairon, C. Salomon, M. Haas, U. D. Jentschura, and C. H. Keitel, New limits on the drift of fundamental constants from laboratory measurements, *Phys. Rev. Lett.* **92**, 230802 (2004).
- [6] R. M. Godun, P. B. R. Nisbet-Jones, J. M. Jones, S. A. King, L. A. M. Johnson, H. S. Margolis, K. Szymaniec, S. N. Lea, K. Bongs, and P. Gill, Frequency ratio of two optical clock transitions in  $^{171}\text{Yb}^+$  and constraints on the time variation of fundamental constants, *Phys. Rev. Lett.* **113**, 210801 (2014).
- [7] J. C. Berengut, D. Budker, C. Delaunay, V. V. Flambaum, C. Frugiuele, E. Fuchs, C. Grojean, R. Harnik, R. Ozeri, G. Perez, and Y. Soreq, Probing new long-range interactions by isotope shift spectroscopy, *Phys. Rev. Lett.* **120**, 091801 (2018).
- [8] I. Counts, J. Hur, D. P. L. Aude Craik, H. Jeon, C. Leung, J. C. Berengut, A. Geddes, A. Kawasaki, W. Jhe, and V. Vuletić, Evidence for nonlinear isotope shift in  $\text{yb}^+$  search for new boson, *Phys. Rev. Lett.* **125**, 123002 (2020).
- [9] C. Solaro, S. Meyer, K. Fisher, J. C. Berengut, E. Fuchs, and M. Drewsen, Improved isotope-shift-based bounds on bosons beyond the standard model through measurements of the  $^2\text{D}_{3/2} - ^2\text{D}_{5/2}$  interval in  $\text{Ca}^+$ , *Phys. Rev. Lett.* **125**, 123003 (2020).
- [10] M. S. Safronova, D. Budker, D. DeMille, D. F. J. Kimball, A. Derevianko, and C. W. Clark, Search for new physics with atoms and molecules, *Rev. Mod. Phys.* **90**, 025008 (2018).
- [11] C. Sanner, N. Huntemann, R. Lange, C. Tamm, E. Peik, M. S. Safronova, and S. G. Porsev, Optical clock comparison for Lorentz symmetry testing, *Nature* **567**, 204 (2019).
- [12] A. D. Ludlow, M. M. Boyd, J. Ye, E. Peik, and P. O. Schmidt, Optical atomic clocks, *Rev. Mod. Phys.* **87**, 637 (2015).
- [13] S. M. Brewer, J.-S. Chen, A. M. Hankin, E. R. Clements, C. W. Chou, D. J. Wineland, D. B. Hume, and D. R. Leibbrandt,  $^{27}\text{Al}^+$  quantum-logic clock with a systematic uncertainty below  $10^{-18}$ , *Phys. Rev. Lett.* **123**, 033201 (2019).
- [14] M. Takamoto, F.-L. Hong, R. Higashi, and H. Katori, An optical lattice clock, *Nature* **435**, 321 (2005).
- [15] A. Yamaguchi, M. S. Safronova, K. Gibble, and H. Katori, Narrow-line cooling and determination of the magic wavelength of  $\text{cd}$ , *Phys. Rev. Lett.* **123**, 113201 (2019).
- [16] N. Ohtsubo, Y. Li, K. Matsubara, N. Nemitz, H. Hachisu, T. Ido, and K. Hayasaka, Optical clock based on a sympathetically-cooled indium ion, *Hyperfine Interact.* **240**, 1 (2019).
- [17] N. D. Lemke, A. D. Ludlow, Z. W. Barber, T. M. Fortier, S. A. Diddams, Y. Jiang, S. R. Jefferts, T. P. Heavner, T. E. Parker, and C. W. Oates, Spin-1/2 optical lattice clock, *Phys. Rev. Lett.* **103**, 063001 (2009).
- [18] J. J. McFerran, L. Yi, S. Mejri, S. Di Manno, W. Zhang, J. Guéna, Y. Le Coq, and S. Bize, Neutral atom frequency reference in the deep ultraviolet with fractional uncertainty =  $5.7 \times 10^{-15}$ , *Phys. Rev. Lett.* **108**, 183004 (2012).
- [19] Y. Huang, H. Guan, P. Liu, W. Bian, L. Ma, K. Liang, T. Li, and K. Gao, Frequency comparison of two  $^{40}\text{Ca}^+$  optical clocks with an uncertainty at the  $10^{-17}$  level, *Phys. Rev. Lett.* **116**, 013001 (2016).
- [20] H. Margolis, G. Barwood, G. Huang, H. Klein, S. Lea, K. Szymaniec, and P. Gill, Hertz-level measurement of the optical clock frequency in a single  $^{88}\text{Sr}^+$  ion, *Science* **306**, 1355 (2004).
- [21] S. A. Diddams, T. Udem, J. Bergquist, E. Curtis, R. Drullinger, L. Hollberg, W. M. Itano, W. Lee, C. Oates, K. Vogel, *et al.*, An optical clock based on a single trapped  $^{199}\text{Hg}^+$  ion, *Science* **293**, 825 (2001).
- [22] V. A. Dzuba, S. O. Allehabi, V. V. Flambaum, J. Li, and S. Schiller, Time keeping and searching for new physics using metastable states of Cu, Ag, and Au, *Phys. Rev. A* **103**, 022822 (2021).
- [23] C. A. Holliman, M. Fan, A. Contractor, S. M. Brewer, and A. M. Jayich, Radium ion optical clock, *Phys. Rev. Lett.* **128**, 033202 (2022).
- [24] K. J. Arnold, R. Kaewuam, A. Roy, E. Paez, S. Wang, and M. D. Barrett, Observation of the  $^1\text{S}_0$  to  $^3\text{D}_1$  clock transition in  $^{175}\text{Lu}^+$ , *Phys. Rev. A* **94**, 052512 (2016).
- [25] R. Kaewuam, T. R. Tan, K. J. Arnold, S. R. Chanu, Z. Zhang, and M. D. Barrett, Hyperfine averaging by dynamic decoupling in a multi-ion lutetium clock, *Phys. Rev. Lett.* **124**, 083202 (2020).
- [26] N. Huntemann, M. Okhapkin, B. Lipphardt, S. Weyers, C. Tamm, and E. Peik, High-accuracy optical clock based on the octupole transition in  $^{171}\text{Yb}^+$ , *Phys. Rev. Lett.* **108**, 090801 (2012).
- [27] H. A. Füst, C.-H. Yeh, D. Kalincev, A. P. Kulosa, L. S. Dreissen, R. Lange, E. Benkler, N. Huntemann, E. Peik, and T. E. Mehlstäubler, Coherent excitation of the highly forbidden electric octupole transition in  $^{172}\text{Yb}^+$ , *Phys. Rev. Lett.* **125**, 163001 (2020).
- [28] K. J. Arnold, R. Kaewuam, A. Roy, T. R. Tan, and M. D. Barrett, Blackbody radiation shift assessment for a lutetium ion clock, *Nat. Commun.* **9**, 1 (2018).
- [29] A. Golovizin, E. Fedorova, D. Tregubov, D. Sukachev, K. Khabarova, V. Sorokin, and N. Kolachevsky, Inner-shell clock transition in atomic thulium with a small blackbody radiation shift, *Nat. Commun.* **10**, 1 (2019).
- [30] N. Huntemann, C. Sanner, B. Lipphardt, C. Tamm, and E. Peik, Single-ion atomic clock with  $3 \times 10^{-18}$  systematic uncertainty, *Phys. Rev. Lett.* **116**, 063001 (2016).
- [31] C. J. Campbell, A. G. Radnaev, A. Kuzmich, V. A. Dzuba, V. V. Flambaum, and A. Derevianko, Single-ion nuclear clock for metrology at the 19th decimal place, *Phys. Rev. Lett.* **108**, 120802 (2012).
- [32] B. Seiferle, L. von der Wense, P. V. Bilous, I. Amersdorfer, C. Lemell, F. Libisch, S. Stellmer, T. Schumm, C. E. Düllmann, A. Pálffy, *et al.*, Energy of the  $^{229}\text{Th}$  nuclear clock transition, *Nature* **573**, 243 (2019).
- [33] K. Beeks, T. Sikorsky, T. Schumm, J. Thielking, M. V.

- Okhapkin, and E. Peik, The thorium-229 low-energy isomer and the nuclear clock, *Nat. Rev. Phys.* **3**, 238 (2021).
- [34] M. Kozlov, M. Safronova, J. R. Crespo López-Urrutia, and P. Schmidt, Highly charged ions: Optical clocks and applications in fundamental physics, *Rev. Mod. Phys.* **90**, 045005 (2018).
- [35] S. A. King, L. J. Spieß, P. Micke, A. Wilzewski, T. Leopold, E. Benkler, R. Lange, N. Huntemann, A. Surzhykov, V. A. Yerokhin, *et al.*, An optical atomic clock based on a highly charged ion, *Nature* **611**, 43 (2022).
- [36] C. Lyu, S. M. Cavaletto, C. H. Keitel, and Z. Harman, Interrogating the temporal coherence of EUV frequency combs with highly charged ions, *Phys. Rev. Lett.* **125**, 093201 (2020).
- [37] B.-B. Suo, Y.-M. Yu, B. K. Sahoo, Highly charged ion (HCI) clocks: Frontier candidates for testing variation of fine-structure constant, arXiv:2211.12162 doi.org/10.48550/arXiv.2211.12162.
- [38] S. Kraemer, J. Moens, M. Athanasakis-Kaklamanakis, S. Bara, K. Beeks, P. Chhetri, K. Chrysalidis, A. Claessens, T. E. Cocolios, J. M. Correia, *et al.*, Observation of the radiative decay of the  $^{229}\text{Th}$  nuclear clock isomer, arXiv preprint arXiv:2209.10276 (2022).
- [39] S. Schiller, Hydrogenlike highly charged ions for tests of the time independence of fundamental constants, *Phys. Rev. Lett.* **98**, 180801 (2007).
- [40] V. I. Yudin, A. V. Taichenachev, and A. Derevianko, Magnetic-dipole transitions in highly charged ions as a basis of ultraprecise optical clocks, *Phys. Rev. Lett.* **113**, 233003 (2014).
- [41] Y.-M. Yu and B. K. Sahoo, Scrutinizing al-like  $^{51}\text{V}^{10+}$ ,  $^{53}\text{Cr}^{11+}$ ,  $^{55}\text{Mn}^{12+}$ ,  $^{57}\text{Fe}^{13+}$ ,  $^{59}\text{Co}^{14+}$ ,  $^{61}\text{Ni}^{15+}$ , and  $^{63}\text{Cu}^{16+}$  ions for atomic clocks with uncertainties below the  $10^{-19}$  level, *Phys. Rev. A* **94**, 062502 (2016).
- [42] A. Windberger, F. Torretti, A. Borschevsky, A. Ryabtsev, S. Dobrodey, H. Bekker, E. Eliav, U. Kaldor, W. Ubachs, R. Hoekstra, J. R. Crespo López-Urrutia, and O. O. Versolato, Analysis of the fine structure of  $\text{Sn}^{11+}$ – $\text{Sn}^{14+}$  ions by optical spectroscopy in an electron-beam ion trap, *Phys. Rev. A* **94**, 012506 (2016).
- [43] P. Micke, T. Leopold, S. King, E. Benkler, L. Spieß, L. Schmoeger, M. Schwarz, J. R. Crespo López-Urrutia, and P. Schmidt, Coherent laser spectroscopy of highly charged ions using quantum logic, *Nature* **578**, 60 (2020).
- [44] N.-H. Rehbehn, M. K. Rosner, H. Bekker, J. C. Berengut, P. O. Schmidt, S. A. King, P. Micke, M. F. Gu, R. Müller, A. Surzhykov, and J. R. Crespo López-Urrutia, Sensitivity to new physics of isotope-shift studies using the coronal lines of highly charged calcium ions, *Phys. Rev. A* **103**, L040801 (2021).
- [45] J. C. Berengut, V. A. Dzuba, and V. V. Flambaum, Enhanced laboratory sensitivity to variation of the fine-structure constant using highly charged ions, *Phys. Rev. Lett.* **105**, 120801 (2010).
- [46] J. C. Berengut, V. A. Dzuba, V. V. Flambaum, and A. Ong, Electron-hole transitions in multiply charged ions for precision laser spectroscopy and searching for variations in  $\alpha$ , *Phys. Rev. Lett.* **106**, 210802 (2011).
- [47] U. I. Safronova, V. V. Flambaum, and M. S. Safronova, Transitions between the  $4f$ -core-excited states in  $\text{Ir}^{16+}$ ,  $\text{Ir}^{17+}$ , and  $\text{Ir}^{18+}$  ions for clock applications, *Phys. Rev. A* **92**, 022501 (2015).
- [48] M. S. Safronova, V. A. Dzuba, V. V. Flambaum, U. I. Safronova, S. G. Porsev, and M. G. Kozlov, Highly charged ions for atomic clocks, quantum information, and search for  $\alpha$  variation, *Phys. Rev. Lett.* **113**, 030801 (2014).
- [49] H. Bekker, A. Borschevsky, Z. Harman, C. Keitel, T. Pfeifer, P. Schmidt, J. R. Crespo López-Urrutia, and J. Berengut, Detection of the  $5p$ – $4f$  orbital crossing and its optical clock transition in  $\text{Pr}^{9+}$ , *Nat. Commun.* **10**, 1 (2019).
- [50] Y.-M. Yu, D. Pan, S. Chen, H. Guan, K. Gao, and J. Chen, Highly charged  $\text{Nd}^{9+}$  ion: A potential candidate of  $\mu\text{Hz}$  linewidth optical clocks for probing fundamental physics, arXiv preprint arXiv:2107.10520 (2021).
- [51] J. C. Berengut, V. A. Dzuba, V. V. Flambaum, and A. Ong, Optical transitions in highly charged californium ions with high sensitivity to variation of the fine-structure constant, *Phys. Rev. Lett.* **109**, 070802 (2012).
- [52] V. Dzuba and V. Flambaum, Highly charged ions for atomic clocks and search for variation of the fine structure constant, in *TCP 2014* (Springer, 2017) pp. 79–86.
- [53] D. K. Nandy and B. K. Sahoo, Highly charged  $\text{W}^{13+}$ ,  $\text{Ir}^{16+}$ , and  $\text{Pt}^{17+}$  ions as promising optical clock candidates for probing variations of the fine-structure constant, *Phys. Rev. A* **94**, 032504 (2016).
- [54] U. Feldman, P. Indelicato, and J. Sugar, Magnetic dipole line from U LXXI ground-term levels predicted at 3200 Å, *J. Opt. Soc. Am. B* **8**, 3 (1991).
- [55] C. A. Morgan, F. G. Serpa, E. Takács, E. S. Meyer, J. D. Gillaspay, J. Sugar, J. R. Roberts, C. M. Brown, and U. Feldman, Observation of visible and uv magnetic dipole transitions in highly charged xenon and barium, *Phys. Rev. Lett.* **74**, 1716 (1995).
- [56] J. R. Crespo López-Urrutia, The visible spectrum of highly charged ions: A window to fundamental physics, *Can. J. Phys.* **86**, 111 (2008).
- [57] P. Micke, S. Kühn, L. Buchauer, J. Harries, T. M. Bücking, K. Blaum, A. Cieluch, A. Egl, D. Hollain, S. Kraemer, *et al.*, The heidelberg compact electron beam ion traps, *Rev. Sci. Instrum.* **89**, 063109 (2018).
- [58] F. Herfurth, Z. Andelkovic, W. Barth, W. Chen, L. Dahl, S. Fedotova, P. Gerhard, M. Kaiser, O. Kester, H. Kluge, *et al.*, The HITRAP facility for slow highly charged ions, *Physica Scripta* **2015**, 014065 (2015).
- [59] X. Yang, S. Wang, S. Wilkins, and R. G. Ruiz, Laser spectroscopy for the study of exotic nuclei, *Prog. Part. Nucl. Phys.* **129**, 104005 (2023).
- [60] S. Malbrunot-Ettenauer, S. Kaufmann, S. Bacca, C. Barbieri, J. Billowes, M. L. Bissell, K. Blaum, B. Cheal, T. Duguet, R. F. G. Ruiz, W. Gins, C. Gorges, G. Hagen, H. Heylen, J. D. Holt, G. R. Jansen, A. Kanellakopoulos, M. Kortelainen, T. Miyagi, P. Navrátil, W. Nazarewicz, R. Neugart, G. Neyens, W. Nörtershäuser, S. J. Novario, T. Papenbrock, T. Ratajczyk, P.-G. Reinhard, L. V. Rodríguez, R. Sánchez, S. Sailer, A. Schwenk, J. Simonis, V. Somà, S. R. Stroberg, L. Wehner, C. Wraith, L. Xie, Z. Y. Xu, X. F. Yang, and D. T. Yordanov, Nuclear charge radii of the nickel isotopes  $^{58-68,70}\text{Ni}$ , *Phys. Rev. Lett.* **128**, 022502 (2022).
- [61] F. Sommer, K. König, D. M. Rossi, N. Everett, D. Garand, R. P. de Groote, J. D. Holt, P. Imgram, A. Incorvati, C. Kalman, A. Klose, J. Lantis, Y. Liu, A. J. Miller, K. Minamisono, T. Miyagi, W. Nazarewicz, W. Nörtershäuser, S. V. Pineda, R. Powel, P.-G. Reinhard, L. Renth, E. Romero-Romero, R. Roth,

- A. Schwenk, C. Sumithrarachchi, and A. Teigelhöfer, Charge radii of  $^{55,56}\text{Ni}$  reveal a surprisingly similar behavior at  $n = 28$  in ca and ni isotopes, *Phys. Rev. Lett.* **129**, 132501 (2022).
- [62] L. V. Rodríguez, D. L. Balabanski, M. L. Bissell, K. Blaum, B. Cheal, G. De Gregorio, J. Ekman, R. F. Garcia Ruiz, A. Gargano, G. Georgiev, W. Gins, C. Gorges, H. Heylen, A. Kanellakopoulos, S. Kaufmann, V. Lagaki, S. Lechner, B. Maaß, S. Malbrunot-Ettenauer, R. Neugart, G. Neyens, W. Nörtershäuser, S. Sailer, R. Sánchez, S. Schmidt, L. Wehner, C. Wraith, L. Xie, Z. Y. Xu, X. F. Yang, and D. T. Yordanov, Doubly-magic character of  $^{132}\text{Sn}$  studied via electromagnetic moments of  $^{133}\text{Sn}$ , *Phys. Rev. C* **102**, 051301 (2020).
- [63] D. T. Yordanov, L. V. Rodríguez, D. L. Balabanski, J. Bieroń, M. L. Bissell, K. Blaum, B. Cheal, J. Ekman, G. Gaigalas, R. F. Garcia Ruiz, *et al.*, Structural trends in atomic nuclei from laser spectroscopy of tin, *Commun. Phys.* **3**, 107 (2020).
- [64] K. Numata, A. Kemery, and J. Camp, Thermal-noise limit in the frequency stabilization of lasers with rigid cavities, *Phys. Rev. Lett.* **93**, 250602 (2004).
- [65] Y. Jiang, A. Ludlow, N. D. Lemke, R. W. Fox, J. A. Sherman, L.-S. Ma, and C. W. Oates, Making optical atomic clocks more stable with  $10^{-16}$ -level laser stabilization, *Nat. Photon.* **5**, 158 (2011).
- [66] D. G. Matei, T. Legero, S. Häfner, C. Grebing, R. Weyrich, W. Zhang, L. Sonderhouse, J. M. Robinson, J. Ye, F. Riehle, and U. Sterr, 1.5  $\mu\text{m}$  lasers with sub-10 mHz linewidth, *Phys. Rev. Lett.* **118**, 263202 (2017).
- [67] D. Kedar, J. Yu, E. Oelker, A. Staron, W. R. Milner, J. M. Robinson, T. Legero, F. Riehle, U. Sterr, and J. Ye, Frequency stability of cryogenic silicon cavities with semiconductor crystalline coatings, *arXiv preprint arXiv:2210.14881* (2022).
- [68] I. Pupeza, S. Holzberger, T. Eidam, H. Carstens, D. Esser, J. Weitenberg, P. Rußbüldt, J. Rauschenberger, J. Limpert, T. Udem, *et al.*, Compact high-repetition-rate source of coherent 100 eV radiation, *Nat. Photon.* **7**, 608 (2013).
- [69] C. Benko, T. K. Allison, A. Cingöz, L. Hua, F. Labaye, D. C. Yost, and J. Ye, Extreme ultraviolet radiation with coherence time greater than 1 s, *Nat. Photon.* **8**, 530 (2014).
- [70] I. P. Grant, *Relativistic quantum theory of atoms and molecules: theory and computation* (Springer, 2007).
- [71] C. F. Fischer, G. Gaigalas, P. Jönsson, and J. Bieroń, GRASP2018—A Fortran 95 version of the general relativistic atomic structure package, *Comput. Phys. Commun.* **237**, 184 (2019).
- [72] K. Kromer, C. Lyu, M. Door, *et al.*, Observation of a low-lying metastable electronic state in highly charged lead by Penning-trap mass spectrometry, In submission.
- [73] Supplemental Materials.
- [74] K. Beloy, V. A. Dzuba, and S. M. Brewer, Quadruply ionized barium as a candidate for a high-accuracy optical clock, *Phys. Rev. Lett.* **125**, 173002 (2020).
- [75] S. O. Allehabi, S. M. Brewer, V. A. Dzuba, V. V. Flambaum, and K. Beloy, High-accuracy optical clocks based on group-16-like highly charged ions, *Phys. Rev. A* **106**, 043101 (2022).
- [76] S. Chen, Z. Zhou, J. Li, T. Zhang, C. Li, T. Shi, Y. Huang, H. Guan, and K. Gao, Precision Measurement of M1 Optical Clock Transition in  $\text{Ni}^{12+}$ , *arXiv:2303.04552* (2023).
- [77] B. J. Sussman, Five ways to the nonresonant dynamic stark effect, *Am. J. Phys.* **79**, 477 (2011).
- [78] M. S. Safronova, M. G. Kozlov, and C. W. Clark, Precision calculation of blackbody radiation shifts for optical frequency metrology, *Phys. Rev. Lett.* **107**, 143006 (2011).
- [79] N. Huntemann, C. Sanner, B. Lipphardt, C. Tamm, and E. Peik, Single-ion atomic clock with  $3 \times 10^{-18}$  systematic uncertainty, *Phys. Rev. Lett.* **116**, 063001 (2016).
- [80] W. R. Johnson, *Atomic structure theory* (Springer, 2007).
- [81] R. X. Schüssler, H. Bekker, M. Braß, H. Cakir, J. R. Crespo López-Urrutia, M. Door, P. Filianin, Z. Harman, M. W. Haverkort, W. J. Huang, *et al.*, Detection of metastable electronic states by penning trap mass spectrometry, *Nature* **581**, 42 (2020).
- [82] R. Lange, N. Huntemann, A. A. Peshkov, A. Surzhykov, and E. Peik, Excitation of an electric octupole transition by twisted light, *Phys. Rev. Lett.* **129**, 253901 (2022).
- [83] J. C. Berengut, C. Delaunay, A. Geddes, and Y. Soreq, Generalized king linearity and new physics searches with isotope shifts, *Phys. Rev. Res.* **2**, 043444 (2020).
- [84] I. Pupeza, C. Zhang, M. Högner, and J. Ye, Extreme-ultraviolet frequency combs for precision metrology and attosecond science, *Nat. Photon.* **15**, 175 (2021).
- [85] J. Nauta, J.-H. Oelmann, A. Borodin, A. Ackermann, P. Knauer, I. Muhammad, R. Pappenberger, T. Pfeifer, and J. C. López-Urrutia, XUV frequency comb production with an astigmatism-compensated enhancement cavity, *Opt. Exp.* **29**, 2624 (2021).
- [86] J. Zhang, L.-Q. Hua, Z. Chen, M.-F. Zhu, C. Gong, and X.-J. Liu, Extreme ultraviolet frequency comb with more than 100  $\mu\text{W}$  average power below 100nm, *Chin. Phys. Lett.* **37**, 124203 (2020).
- [87] L. S. Dreissen, C. Roth, E. L. Gründeman, J. J. Krauth, M. Favier, and K. S. E. Eikema, High-precision ramsey-comb spectroscopy based on high-harmonic generation, *Phys. Rev. Lett.* **123**, 143001 (2019).
- [88] C. Lyu, C. H. Keitel, and Z. Harman, In preparation,.

## I. SUPPLEMENTAL MATERIALS

This material summarizes the mixing coefficients for low-lying states in selected  $4d^6$ ,  $4d^5$ , and  $4d^4$  ions. For heavy elements, the strong relativistic effect leads to large splittings between the  $4d_{3/2}$  and  $4d_{5/2}$  relativistic orbitals, with the subscripts being the corresponding single-electron total angular momenta. As the atomic number  $Z$  increases, the energies of atomic states dominated by the  $4d_{3/2}$  orbital scale much slower than those of the states involving high fraction of the  $4d_{5/2}$  orbital. This impropotional scaling effect leads to the reordering of fine-structure terms, thus the emergence of metastable states. The notation  $4d_{3/2}^2(0)$  means there are 2 electrons in the  $4d_{3/2}$  orbital, and the total angular momentum of these two electrons is 0.

### I.1. $4d^6$ ions

For Mo and Mo-like  $\text{Sn}^{8+}$ , the ASFs are dominated by the  $4d_{3/2}^3(3/2)4d_{5/2}^3(3/2)$  configuration where  $d_{3/2}$  and  $d_{5/2}$  orbitals are equally occupied. However, for  $\text{U}^{50+}$ , the energy of the  $4d_{3/2}$  orbital is 55.8 eV lower than that of the  $4d_{5/2}$  orbital. Thus, the dominate CSFs, for the low-lying  $J = 0, 2, 4$  states, are given by  $4d_{3/2}^4(0)4d_{5/2}^2(0)$ ,  $4d_{3/2}^4(0)4d_{5/2}^2(4)$ , and  $4d_{3/2}^4(0)4d_{5/2}^2(4)_{5/2}$ , respectively. However, the  $4d_{3/2}^4 4d_{5/2}^2$  configuration does not allow angular coupling with  $J = 1, 3$ . Therefore, the terms with  $J = 1, 3$  have more electrons occupying the  $4d_{5/2}$  orbital, and thus will have much higher energy than the other three terms. Similar analysis also applies to the  $4d^5$  and  $4d^4$  ions shown in Sec. I.2 and I.3, respectively.

Table 2. Absolute binding energies of the  $4d_{3/2}$  and  $4d_{5/2}$  relativistic orbitals in  $4d^6$  ions.

ion	$E_{4d_{3/2}}$ (a.u.)	$E_{4d_{5/2}}$ (a.u.)	$\Delta E$ (eV)
42Mo <sup>0+</sup>	0.214	0.207	0.190
50Sn <sup>8+</sup>	5.916	5.866	1.361
92U <sup>50+</sup>	107.599	105.548	55.811

Table 3. CSF components of the low-lying  $J = 0$  state.

ion	ASF	$c_k$				
42Mo <sup>0+</sup>	0 +	0.76080	0.37843	-0.35227	0.28425	0.27035
		3	1	2	5	4
50Sn <sup>8+</sup>	0 +	0.74400	0.37938	0.36036	-0.32716	0.25620
		3	5	4	2	1
92U <sup>50+</sup>	0 +	0.98227	0.16656	-0.07640	0.03946	0.00383
		5	4	2	3	1
CSF		1	2	3	4	5
		$4d^6(0)_{5/2}$	$4d_{3/2}^2(0)4d_{5/2}^4(0)$	$4d_{3/2}^2(2)4d_{5/2}^4(2)$	$4d_{3/2}^3(3/2)4d_{5/2}^3(3/2)$	$4d_{3/2}^4(0)4d_{5/2}^2(0)$

Table 4. CSF components of the state with  $J = 1$ .

ion	ASF	$c_k$			
42Mo <sup>0+</sup>	1 +	0.64164	-0.51824	-0.41117	-0.38816
		1	3	4	2
50Sn <sup>8+</sup>	1 +	0.57585	0.50747	-0.50443	0.39550
		3	4	1	2
92U <sup>50+</sup>	1 +	0.79804	0.59318	0.09266	-0.05178
		4	3	2	1
CSF		1	2	3	4
		$4d_{3/2}(3/2)4d_{5/2}^5(5/2)$	$4d_{3/2}^2(2)4d_{5/2}^4(2)$	$4d_{3/2}^3(3/2)4d_{5/2}^3(5/2)$	$4d_{3/2}^3(3/2)4d_{5/2}^3(3/2)$



Table 5. CSF components of the state with  $J = 2$ .

ion	ASF	$c_k$				
42Mo <sup>0+</sup>	2 +	0.72324	0.37426	-0.32648	-0.30319	-0.27253
	5		1	8	6	4
50Sn <sup>8+</sup>	2 +	0.62622	-0.49708	-0.35745	0.29182	-0.26834
	5		8	6	1	4
92U <sup>50+</sup>	2 +	0.99339	0.09839	-0.03938	0.03373	-0.02196
	8		6	2	7	5
CSF	1					
	5	$4d_{3/2}(3/2)4d_{5/2}^5(5/2)$	$4d_{3/2}^2(0)4d_{5/2}^4(2)$	$4d_{3/2}^2(2)4d_{5/2}^4(0)$	$4d_{3/2}^2(2)4d_{5/2}^4(2)$	
	6					
	8	$4d_{3/2}^2(2)4d_{5/2}^4(4)$	$4d_{3/2}^3(3/2)4d_{5/2}^3(5/2)$	$4d_{3/2}^3(3/2)4d_{5/2}^3(3/2)$	$4d_{3/2}^4(0)4d_{5/2}^2(2)$	

Table 6. CSF components of the state with  $J = 3$ .

ion	ASF	$c_k$				
42Mo <sup>0+</sup>	3 +	0.74515	-0.56412	0.22897	-0.20396	-0.14349
	6		3	4	1	5
50Sn <sup>8+</sup>	3 +	0.74515	-0.56412	0.22897	-0.20396	-0.14349
	6		3	4	1	5
92U <sup>50+</sup>	3 +	0.89099	0.32023	-0.30164	-0.10551	0.02863
	6		4	5	3	2
CSF	1					
	5	$4d_{3/2}(3/2)4d_{5/2}^5(5/2)$	$4d_{3/2}^2(2)4d_{5/2}^4(2)$	$4d_{3/2}^2(2)4d_{5/2}^4(4)$	$4d_{3/2}^3(3/2)4d_{5/2}^3(5/2)$	
	6					
	8	$4d_{3/2}^3(3/2)4d_{5/2}^3(3/2)$	$4d_{3/2}^3(3/2)4d_{5/2}^3(9/2)$			

Table 7. CSF components of the state with  $J = 4$ .

ion	ASF	$c_k$				
42Mo <sup>0+</sup>	4 +	0.67191	0.47875	-0.40263	-0.29717	-0.18941
	6		7	4	2	1
50Sn <sup>8+</sup>	4 +	0.65905	0.59695	-0.31364	-0.26429	0.13655
	6		7	4	2	5
92U <sup>50+</sup>	4 +	0.99493	0.08798	-0.04455	-0.01577	-0.01165
	7		6	2	4	3
CSF	1					
	5	$4d_{3/2}(3/2)4d_{5/2}^5(5/2)$	$4d_{3/2}^2(0)4d_{5/2}^4(4)$	$4d_{3/2}^2(2)4d_{5/2}^4(2)$	$4d_{3/2}^2(2)4d_{5/2}^4(4)$	
	6					
	7	$4d_{3/2}^3(3/2)4d_{5/2}^3(5/2)$	$4d_{3/2}^3(3/2)4d_{5/2}^3(9/2)$	$4d_{3/2}^4(0)4d_{5/2}^2(4)$		

I.2.  $4d^5$  ionsTable 8. Absolute binding energies of the  $4d_{3/2}$  and  $4d_{5/2}$  relativistic orbitals in  $4d_{5/2}^5$  ions.

ion	$\bar{E}_{4d_{3/2}}$ (a.u.)	$\bar{E}_{4d_{5/2}}$ (a.u.)	$\Delta E$ (eV)
42Mo <sup>0+</sup>	0.554	0.547	0.190
50Sn <sup>8+</sup>	6.758	6.706	1.145
92U <sup>50+</sup>	110.328	108.162	58.940

Table 9. CSF components of the ground state with  $J = 5/2$ .

ion	ASF	$c_k$				
42Mo <sup>+</sup>	5/2 +	0.61759	0.50663	-0.45259	0.21928	-0.19577
		7	9	3	10	4
50Sn <sup>9+</sup>	5/2 +	0.58952	0.57196	-0.37560	0.29939	-0.19366
		7	9	3	10	4
92U <sup>51+</sup>	5/2 +	0.99305	0.09767	-0.05647	0.02543	0.01799
		10	9	4	7	6
CSF		1	2	3	4	5
		$4d_{5/2}^5(5/2)$	$4d_{3/2}(3/2)4d_{5/2}^4(2)$	$4d_{3/2}(3/2)4d_{5/2}^4(4)$	$4d_{3/2}^2(0)4d_{5/2}^3(5/2)$	$4d_{3/2}^2(2)4d_{5/2}^3(5/2)$
		6	7	8	9	10
		$4d_{3/2}^2(2)4d_{5/2}^3(3/2)$	$4d_{3/2}^2(2)4d_{5/2}^3(9/2)$	$4d_{3/2}^3(3/2)4d_{5/2}^2(2)$	$4d_{3/2}^3(3/2)4d_{5/2}^2(4)$	$4d_{3/2}^4(0)4d_{5/2}(5/2)$

Table 10. CSF components of the excited state with  $J = 5/2$ .

ion	ASF	$c_k$				
42Mo <sup>+</sup>	5/2 +	0.49676	-0.43361	0.35679	-0.31041	0.29820
		6	8	2	9	7
50Sn <sup>9+</sup>	5/2 +	0.68269	0.39504	-0.36717	0.27866	-0.24829
		10	6	8	3	9
92U <sup>51+</sup>	5/2 +	0.87733	0.45249	0.11797	-0.08731	-0.05064
		9	8	7	10	3
CSF		1	2	3	4	5
		$4d_{5/2}^5(5/2)$	$4d_{3/2}(3/2)4d_{5/2}^4(2)$	$4d_{3/2}(3/2)4d_{5/2}^4(4)$	$4d_{3/2}^2(0)4d_{5/2}^3(5/2)$	$4d_{3/2}^2(2)4d_{5/2}^3(5/2)$
		6	7	8	9	10
		$4d_{3/2}^2(2)4d_{5/2}^3(3/2)$	$4d_{3/2}^2(2)4d_{5/2}^3(9/2)$	$4d_{3/2}^3(3/2)4d_{5/2}^2(2)$	$4d_{3/2}^3(3/2)4d_{5/2}^2(4)$	$4d_{3/2}^4(0)4d_{5/2}(5/2)$

Table 11. CSF components of the excited state with  $J = 7/2$ .

ion	ASF	$c_k$				
42Mo <sup>+</sup>	7/2 +	0.59145	-0.47959	0.39208	-0.32789	0.28363
		5	7	2	6	4
50Sn <sup>9+</sup>	7/2 +	0.65387	-0.46013	0.38918	-0.31272	-0.24884
		7	5	6	2	4
92U <sup>51+</sup>	7/2 +	0.92695	0.37150	-0.03240	-0.02816	-0.02348
		7	6	2	4	1
CSF		1	2	3	4	5
		$4d_{3/2}(3/2)4d_{5/2}^4(2)$	$4d_{3/2}(3/2)4d_{5/2}^4(4)$	$4d_{3/2}^2(2)4d_{5/2}^3(5/2)$	$4d_{3/2}^2(2)4d_{5/2}^3(3/2)$	$4d_{3/2}^2(2)4d_{5/2}^3(9/2)$
		6	7			
		$4d_{3/2}^3(3/2)4d_{5/2}^2(2)$	$4d_{3/2}^3(3/2)4d_{5/2}^2(4)$			

Table 12. CSF components of the state with  $J = 9/2$ .

ion	ASF	$c_k$				
42Mo <sup>+</sup>	9/2 +	0.81369	-0.44351	0.37558	0.01020	0.00565
	4		5	1	2	3
50Sn <sup>9+</sup>	9/2 +	0.77477	-0.55675	0.29631	0.03996	0.01902
	4		5	1	2	3
92U <sup>51+</sup>	9/2 +	0.99487	-0.08321	-0.04440	-0.02742	-0.02423
	5		4	2	3	1
CSF		1 $4d_{3/2}(3/2)4d_{5/2}^4(4)$	2 $4d_{3/2}^2(0)4d_{5/2}^3(9/2)$	3 $4d_{3/2}^2(2)4d_{5/2}^3(5/2)$	4 $4d_{3/2}^2(2)4d_{5/2}^3(9/2)$	5 $4d_{3/2}^3(3/2)4d_{5/2}^2(4)$

Table 13. CSF components of the state with  $J = 11/2$ .

ion	ASF	$c_k$		
42Mo <sup>+</sup>	11/2 +	0.71539	-0.53453	0.44999
	2		3	1
50Sn <sup>9+</sup>	11/2 +	0.67722	-0.64170	-0.35999
	3		2	1
92U <sup>51+</sup>	11/2 +	0.99809	-0.04816	-0.03862
	3		2	1
CSF		1 $4d_{3/2}(3/2)4d_{5/2}^4(4)$	2 $4d_{3/2}^2(2)4d_{5/2}^3(9/2)$	3 $4d_{3/2}^3(3/2)4d_{5/2}^2(4)$

I.3.  $4d^4$  ionsTable 14. Absolute binding energies of the  $4d_{3/2}$  and  $4d_{5/2}$  relativistic orbitals in  $4d_{5/2}^4$  ions.

ion	$E_{4d_{3/2}}$ (a.u.)	$E_{4d_{5/2}}$ (a.u.)	$\Delta E$ (eV)
$42\text{Mo}^{0+}$	0.968	0.960	0.218
$50\text{Sn}^{8+}$	7.628	7.574	1.469
$92\text{U}^{50+}$	113.079	110.888	59.620

Table 15. CSF components of the state with  $J = 0$ .

ion	ASF	$c_k$				
$42\text{Mo}^{2+}$	0 +	0.72165	0.51071	-0.36020	0.22064	0.19994
		4	5	3	1	2
$50\text{Sn}^{10+}$	0 +	0.71207	0.58598	-0.34109	0.14457	0.11108
		5	4	3	1	2
$92\text{U}^{52+}$	0 +	0.99720	-0.06621	0.03466	0.00303	-0.00088
		5	3	4	1	2
CSF		1	2	3	4	5
		$4d_{5/2}^4(0)$	$4d_{3/2}(3/2)4d_{5/2}^3(3/2)$	$4d_{3/2}^2(0)4d_{5/2}^2(0)$	$4d_{3/2}^2(2)4d_{5/2}^2(2)$	$4d_{3/2}^4(0)$

Table 16. CSF components of the state with  $J = 1$ .

ion	ASF	$c_k$			
$42\text{Mo}^{2+}$	1 +	0.74455	-0.45667	0.35526	0.33301
		4	1	3	2
$50\text{Sn}^{10+}$	1 +	0.84828	-0.36950	0.29390	0.23983
		4	1	3	2
$92\text{U}^{52+}$	1 +	0.99761	-0.05523	0.03652	0.01960
		4	1	3	2
CSF		1	2	3	4
		$4d_{3/2}(3/2)4d_{5/2}^3(5/2)$	$4d_{3/2}(3/2)4d_{5/2}^3(3/2)$	$4d_{3/2}^2(2)4d_{5/2}^2(2)$	$4d_{3/2}^3(3/2)4d_{5/2}(5/2)$

Table 17. CSF components of the state with  $J = 2$ .

ion	ASF	$c_k$				
$42\text{Mo}^{2+}$	2 +	0.75176	-0.42854	0.26385	-0.26042	0.24193
		7	8	2	6	1
$50\text{Sn}^{10+}$	2 +	0.75312	-0.50378	-0.23758	0.22462	-0.18064
		7	8	6	2	4
$92\text{U}^{52+}$	2 +	0.98830	-0.14298	-0.04338	0.02404	0.01494
		8	7	2	5	3
CSF		1	2	3	4	
		$4d_{5/2}^4(2)$	$4d_{3/2}(3/2)4d_{5/2}^3(5/2)$	$4d_{3/2}(3/2)4d_{5/2}^3(3/2)$	$4d_{3/2}^2(0)4d_{5/2}^2(2)$	
		5	6	7	8	
		$4d_{3/2}^2(2)4d_{5/2}^2(0)$	$4d_{3/2}^2(2)4d_{5/2}^2(2)$	$4d_{3/2}^2(2)4d_{5/2}^2(4)$	$4d_{3/2}^3(3/2)4d_{5/2}(5/2)$	

Table 18. CSF components of the state with  $J = 3$ .

ion	ASF	$c_k$				
42Mo <sup>2+</sup>	3 +	0.67715	-0.62242	-0.31231	0.19152	-0.10257
	5		3	6	1	4
50Sn <sup>10+</sup>	3 +	0.71626	-0.53100	-0.40474	0.17041	-0.08183
	5		3	6	1	4
92U <sup>52+</sup>	3 +	0.99140	-0.11531	-0.04676	-0.03413	0.01854
	6		5	4	1	3
CSF	1		2	3	4	
	4d <sub>3/2</sub> (3/2)4d <sub>5/2</sub> <sup>3</sup> (5/2)	4d <sub>3/2</sub> (3/2)4d <sub>5/2</sub> <sup>3</sup> (3/2)	4d <sub>3/2</sub> (3/2)4d <sub>5/2</sub> <sup>3</sup> (9/2)	4d <sub>3/2</sub> (2)4d <sub>5/2</sub> <sup>2</sup> (2)		
	5	6				
	4d <sub>3/2</sub> <sup>2</sup> (2)4d <sub>5/2</sub> <sup>2</sup> (4)	4d <sub>3/2</sub> <sup>3</sup> (3/2)4d <sub>5/2</sub> (5/2)				

Table 19. CSF components of the state with  $J = 4$ .

ion	ASF	$c_k$				
42Mo <sup>2+</sup>	4 +	0.64516	-0.46912	-0.39396	0.32122	0.25876
	3		6	1	4	7
50Sn <sup>10+</sup>	4 +	0.55959	-0.52906	0.40707	0.33947	-0.28611
	3		6	7	4	1
92U <sup>52+</sup>	4 +	0.99728	-0.04564	0.04427	-0.02746	0.01816
	7		2	4	6	5
CSF	1		2	3	4	
	4d <sub>5/2</sub> <sup>4</sup> (4)	4d <sub>3/2</sub> (3/2)4d <sub>5/2</sub> <sup>3</sup> (5/2)	4d <sub>3/2</sub> (3/2)4d <sub>5/2</sub> <sup>3</sup> (9/2)	4d <sub>3/2</sub> <sup>2</sup> (2)4d <sub>5/2</sub> <sup>2</sup> (4)		
	5	6	7			
	4d <sub>3/2</sub> <sup>2</sup> (2)4d <sub>5/2</sub> <sup>2</sup> (2)	4d <sub>3/2</sub> <sup>2</sup> (2)4d <sub>5/2</sub> <sup>2</sup> (4)	4d <sub>3/2</sub> <sup>3</sup> (3/2)4d <sub>5/2</sub> (5/2)			